Progress In Electromagnetics Research C, Vol. 98, 109–125, 2020

Retrieval of Tropical Peatland Forest Biomass from Polarimetric Features in Central Kalimantan, Indonesia

Mirza Muhammad Waqar[1, *], Rahmi Sukmawati[2], Yaqi Ji[1], Josaphat Tetuko Sri Sumantyo[1], Hendrik Segah[3], and Lilik Budi Prasetyo[4]

Abstract—In this research, the potential of L-band SAR data is evaluated for tropical peatland forest biomass estimation using polarimetric features and field data. For this, ALOS-2 full polarimetric data are acquired over central Kalimantan, Indonesia. Total 54 sampled plots ($20\,\mathrm{m} \times 20\,\mathrm{m}$) were established in the study site; diameter at breast height (DBH) and tree species of every tree were collected in each plot. Locally developed allometric equations were used to convert field data to biomass and plot level biomass, and the upscaling factor was applied to upscale plot level biomass to standard tones per hectare scale. Backscattering coefficient (σ_o) was computed for HH, HV, VH and VV polarization. Similarly, eigen decomposition was performed to extract: entropy (E), alpha (α), and anisotropy (A); also diversity indices were computed. Yamaguchi decomposition was performed to extract scattering behavior of forest in central Kalimantan. All polarimetric parameters were upscaled to one-hectare scale. Field data were divided into training plots (70 percent $\rightarrow$ 42 plots) and validation plots (30 percent $\rightarrow$ 12 plots). Nonlinear regression analysis was performed between polarimetric parameters and training plots. Perplexity, Shannon index, entropy, Gini Simpson index, index of qualitative inversion, Reyni entropy (order 2), σ_{HV}, alpha, σ_{VV}, and volumetric scattering component were found significantly correlated (ranging R^2 from 0.67 to 0.49) with the field data. The corresponding nonlinear model was inverted, and biomass maps were computed for the individual model. The resultant biomass maps were validated using a validation set of referenced measurements. Perplexity, Shannon index, entropy, Gini Simpson index, index of qualitative inversion, Reyni entropy (order 2), σ_{HV}, alpha, σ_{VV}, and volumetric scattering exhibited a significant correlation between field biomass and predicted biomass computed using developed model. R^2 for validation ranges from 0.95 to 0.81 with RMSE ranging from $13.59\,\mathrm{Mgha}^{-1}$ to $25.63\,\mathrm{Mgha}^{-1}$. The estimated biomass in study site ranges from $49.31\,\mathrm{Mgha}^{-1}$ to $290.60\,\mathrm{Mgha}^{-1}$.

1. INTRODUCTION

Tropical forest is playing an important role in carbon balancing by removing CO_2 from the atmosphere by the process of photosynthesis and storing it in terms of forest biomass. This carbon can return to the atmosphere by forest burning, degradation, and deforestation. Hence, it is important to estimate forest biomass at the regional scale to understand the carbon cycle over that area. Tropical forest is the most significant terrestrial reservoir for carbon. The Indonesian rain forest is home to 10–15 percent of the world's known plants, mammals, and birds. Due to commercial activities, forest burning, deforestation, and degradation, Indonesia has lost 72 percent of its intact forest. The forest cover in

Received 28 August 2019, Accepted 15 December 2019, Scheduled 31 December 2019
* Corresponding author: Mirza Muhammad Waqar (mirzawaqar@chiba-u.jp).
[1] Center for Environmental Remote Sensing (CEReS), Chiba University, 1-33 Yayoi, Inage, Chiba 263-8522, Japan. [2] Padang State University, Jalan, Air Tawar Padang, Sumatera Barat 25111, Indonesia. [3] Universitas Palangka Raya, Kampus Tunjung Nyaho Jalan Yos Sudarso, Palangka Raya, Kalimantan Tengah 73111, Indonesia. [4] Bogor Agricultural University, Jl. Raya Dramaga Kampus IPB Dramaga Bogor, West Java 16680, Indonesia.

Kalimantan, Indonesia is 25.5 million hectares (estimated in 2010). It is essential to determine the current biomass status of forest in Kalimantan to understand regional carbon cycle in a better way. Previously, traditional techniques were used for forest inventory and biomass estimation; this required extensive field work with substantial human resources in the field, and for developing countries, such practices are not sustainable. Recently, remote sensing is being used extensively for forest studies. However, incorporating forest biophysical parameters collected in the field oversampled area increases the accuracy of forest parameter estimation using remote sensing dataset. As tropical regions are mostly covered with clouds, the application of optical remote sensing data is limited over the tropical area. However, synthetic aperture radar (SAR) exhibits excellent potential for forest biophysical parameters estimation over tropical region due to its penetration capability through clouds.

Among other terrestrial carbon pools, forests store CO_2 in its roots, stems, branches, and leaves which are collectively known as forest biomass [1]. Forest biomass is categorized into two categories: 1) above ground biomass (AGB) and 2) below ground biomass (BGB). Using remote sensing techniques, AGB can be estimated effectively. The canopy AGB can be calculated using optical remote sensing because it only gives information of canopy structure, and lidar data give information of vertical forest profile; however, synthetic aperture radar (SAR) provides information of leaves, branches, stems, and soil depending upon wavelength used for SAR imaging. As X-band mostly interacts with leaves and small branches, C-band can penetrate through leaves and main branches, L-band can penetrate through stem of tree and P-band can penetrate through soil cover. This penetration also depends upon the amount of moisture and dielectric constant. However, the estimation of aboveground biomass using remote sensing dataset requires extensive field-based referenced biomass measurements to develop the model between parameters extracted from satellite data and reference biomass measurements.

Researchers attempted to estimate forest AGB using optical, lidar, and SAR datasets. Each of them has potential to estimate different properties of forest structure. Many researchers have used vegetation indices extracted from Landsat to estimate aboveground biomass [2–4], but the key problem is saturation over very low biomass. Mutanga et al. used high resolution worldview-2 dataset for forest biomass estimation using regression analysis between ground data and parameters extracted using high resolution data [5]. Drake et al. used lidar data to map vertical structure and related it with forest biomass [10]. SAR backscattering is also effectively used for forest biomass estimation [6–9].

Urbazaev et al. (2018) and Shao and Zhang (2016) estimated aboveground biomass by developing synergy between field measurements and parameters extracted from SAR, lidar, and optical datset [11, 12]. However, AGB estimation using SAR is limited due to SAR signal saturation at certain biomass threshold. The sensitivity of L-band SAR backscatter to AGB saturates at around 100–150 Mgha^{-1} [6, 37]. However, some researchers find saturation values of more than 250 Mgha^{-1} for L-band [50], to 300 Mgha^{-1} when using multi-frequency SAR datasets such as C- and X-bands [39]. However, there is no current satellite sensor in orbit that provides biomass estimation over tropical forest ($> 400\,\mathrm{Mgha}^{-1}$) with reasonable accuracy [6, 38, 40–43]. A P-band SAR such as a planned BIOMASS mission is needed to retrieve very high AGB [44]. It is also identified that slope is the dominant factor that affects the accuracy of above ground biomass estimation [10].

The main goal of this research is to estimate aboveground biomass in tropical peatland forest using backscatter, polarimetric parameters, and diversity indices.

1.1. Novel Contribution

Recently, many researchers have found that forest diversity is positively linked with aboveground biomass [45–49]. However, the quantitative relationship between AGB and structure — species diversity is poorly understood. The research presented in this paper has made the following contributions to the state of art:

(i) Diversity indices are exploited to link with forest aboveground biomass.

(ii) Polarimetric parameters are used in synergy with field data for accurate estimation of forest aboveground biomass.

2. MAIN POLSAR CONCEPTS IN THE CONTEXT OF THIS STUDY

Fully polarimetric SAR measurements can be represented by scattering matrix shown in the equation below:

$$[S] = \begin{bmatrix} S_{HH} & S_{HV} \\ S_{VH} & S_{VV} \end{bmatrix} \tag{1}$$

where S_{xy} is the complex backscattering term associated with x and y being the transmitted and received polarizations, respectively. Equation (1) can be rewritten in Pauli basis:

$$\vec{k} = \frac{1}{\sqrt{2}} \begin{bmatrix} S_{HH} + S_{VV} & S_{HH} - S_{VV} & 2S_{HV} \end{bmatrix}^T \tag{2}$$

In space-born SAR polarimetry, after polarimetric calibration, Faraday rotation compensation needs to be applied by rotating it an angle θ around the radar line of sight leading to:

$$S' = \begin{bmatrix} \cos\theta & \sin\theta \\ -\sin\theta & \cos\theta \end{bmatrix} \begin{bmatrix} S_{HH} & S_{HV} \\ S_{VH} & S_{VV} \end{bmatrix} \begin{bmatrix} \cos\theta & -\sin\theta \\ \sin\theta & \cos\theta \end{bmatrix} \tag{3}$$

where

$$S' = \begin{bmatrix} S_{hh} & S_{hv} \\ S_{vh} & S_{vv} \end{bmatrix} \tag{4}$$

The corresponding covariance matrix is positive semi-definite Hermittian:

$$[C_3] = \begin{bmatrix} \langle S_{hh} S_{hh}^* \rangle & \left\langle \sqrt{2} S_{hh} S_{hv}^* \right\rangle & \langle S_{hh} S_{hv}^* \rangle \\ \left\langle \sqrt{2} S_{hv} S_{hh}^* \right\rangle & \langle 2 S_{hv} S_{hv}^* \rangle & \left\langle \sqrt{2} S_{hv} S_{vv}^* \right\rangle \\ \langle S_{vv} S_{hh}^* \rangle & \left\langle \sqrt{2} S_{vv} S_{hv}^* \right\rangle & \langle S_{vv} S_{vv}^* \rangle \end{bmatrix} \tag{5}$$

The covariance matrix is fundamental to characterizing SAR image to corresponding scattering components, e.g., surface, double-bounce, and volume scattering. Cloude and Pottier have proposed a polarimetric coherence matrix, reformulating the covariance matrix in the Pauli basis, with the target vector in the reciprocal mono-static case given by Equation (2). Then, the coherence matrix can be expressed as follows:

$$[T_3] = \frac{1}{2} \begin{bmatrix} \left\langle |S_{hh} + S_{vv}|^2 \right\rangle & \langle (S_{hh} + S_{vv})(S_{hh} - S_{vv})^* \rangle & \langle 2(S_{hh} + S_{vv}) S_{hv}^* \rangle \\ \langle (S_{hh} - S_{vv})(S_{hh} + S_{vv})^* \rangle & \left\langle |S_{hh} - S_{vv}|^2 \right\rangle & \langle 2(S_{hh} - S_{vv}) S_{hv}^* \rangle \\ \langle 2 S_{hv} (S_{hh} + S_{vv})^* \rangle & \langle 2 S_{hv} (S_{hh} - S_{vv})^* \rangle & \left\langle 4 |S_{hv}|^2 \right\rangle \end{bmatrix} \tag{6}$$

Yamaguchi Decomposition Parameters Yamaguchi et al. proposed four-component decomposition scheme [13]; this can decompose coherency matrix to the surface, double-bounce, volume, and helix scattering. Mathematical expressions to compute surface and volumetric scattering coefficients are listed below:

$$\gamma_s = \tfrac{1}{2} \left\langle |S_{HH} + S_{VV}|^2 \right\rangle - 4 \left\langle |S_{HV}|^2 \right\rangle + 2 \left| \mathrm{Im} \langle S_{HV}^* (S_{HH} - S_{VV}) \rangle \right| \tag{7}$$

$$\gamma_v = 8 \left\langle |S_{HV}|^2 \right\rangle - 4 \left| \mathrm{Im} \langle S_{HV}^* (S_{HH} - S_{VV}) \rangle \right| \tag{8}$$

Corresponding surface and volumetric scattering power can be obtained by:

$$P_s = \gamma_s (1 + |\beta|^2); \quad P_v = \gamma_v \tag{9}$$

Eigen Decomposition Parameters Cloude and Pottier (1996) proposed the following description for the eigen vectors of the covariance matrix in Pauli basis [14]:

$$\tilde{e} = \begin{bmatrix} \cos\alpha & \sin\alpha \cos\beta e^{i\delta} & \sin\alpha \sin\beta e^{i\gamma} \end{bmatrix} \tag{10}$$

The average angle α can be calculated using

$$Alpha(\alpha) = P_1 \lambda_1 + P_2 \lambda_2 + P_3 \lambda_3 \tag{11}$$

where

$$\lambda_1 = \frac{1}{2}\left|S_{HH} + S_{VV}\right|^2 \tag{12}$$

$$\lambda_2 = \frac{1}{4}\left|S_{HH} - S_{VV}\right|^2 + \left|S_{HV}\right|^2 + \mathrm{Im}S^*_{HV}(\left|S_{HH} - S_{VV}\right|^2) \tag{13}$$

$$\lambda_3 = \frac{1}{4}\left|S_{HH} - S_{VV}\right|^2 + \left|S_{HV}\right|^2 - \mathrm{Im}S^*_{HV}(\left|S_{HH} - S_{VV}\right|^2) \tag{14}$$

Entropy is the measure of target randomness or disorder, which is defined as:

$$Entropy(H) = -\sum_{i=1}^{3} p_i \cdot \log_3(p_i); \quad p_i = \frac{\lambda_i}{\sum_{k=1}^{3} \lambda_k} \tag{15}$$

Similarly, anisotropy can be defined as:

$$Anisotropy(A) = \frac{\lambda_2 - \lambda_3}{\lambda_2 + \lambda_3} \tag{16}$$

Backscattering Coefficient The radar backscattering coefficient σ^o provides information about the imaging surface, and it is the function of radar observation parameters: frequency, polarization, incident angle, and surface parameters: roughness, geometric shape, and dielectric constant of the target.

$$\sigma^o_{slc} = 10 \cdot \log_{10}\left\langle I^2 + Q^2 \right\rangle + CF_1 + A \tag{17}$$

where σ^o is the backscattering coefficient (sigma naught or sigma zero, units in dB), and $CF_1 = -83$ [units: dB] and $A = 32$ [units: dB] are calibration factors, respectively [15–17].

Diversity Index A diversity index reflects how many different species exist in a given dataset, and it also considers how evenly different species are distributed in the dataset. It also explains diversity, richness, and abundance in the given set of data. The expressions for Shannon index, Simpson index, Reyni Entropy, Gini Simpson Index, and perplexity are given as below:

$$Shannon\,Index = -\sum_{i=1}^{n} p_i \cdot \ln(p_i) \tag{18}$$

$$Simpson\,Index = \frac{1}{\sum_{i=1}^{n} p_i^2} \tag{19}$$

where p is the proportion (n/N) of individuals of one particular species found (n) divided by the total number of individuals found (N).

$$Gini\,Simpson\,Index = 1 - \sum_{i=1}^{n} p_i^2 \tag{20}$$

The Renyi entropy of order q, where $q \geq 0$ and $q \neq 1$, is defined as:

$$Reyni\,Entropy = \frac{1}{1-q} \cdot \ln\left(\sum_{i=1}^{n} p_i^q\right) \tag{21}$$

$$Perplexity = \exp\left(-\frac{1}{N}\log(p(x))\right) \tag{22}$$

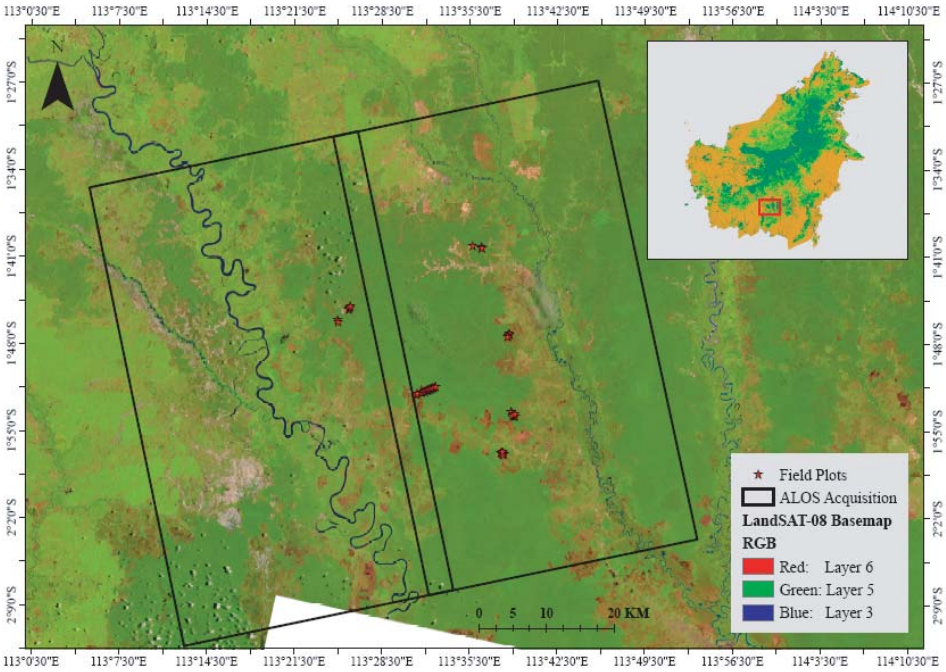

Figure 1. Location of the study area.

3. DATA AND METHOD

3.1. Study Area

The study site is located in tropical peat and kerangas forests around Palangkaraya, the capital city of Central Kalimantan Province, Indonesia (Figure 1). Central Kalimantan lies within the Inter-Tropical Convergence Zone (ITCZ), and it falls under the wet tropical climate region. Central Kalimantan is hot and humid, and the mean daily temperature ranges from 24C° to 30C°. Annual rainfall varies between 2,500 and 2,800 mm [18–20]. Rainfall in study area is common throughout the year; however, October to February is the rainy season, and March to September are dry months. The forest canopy has three strata with a maximum height of 35 m. The principal tree species of the upper canopy are Gonystylus Bancanus, Shorea spp. (Meranti), Cratoxylon Glaucum (Gerongang), and Dactylocladus Stenostachys (Mentibu). The mix swamp forest grades into the low-pole forest, which continues for a further 7 km from Sebangau river or so. Low canopy forest has only two strata and very few trees of commercial value. The principal species of the upper canopy are Combretocarpus Rotundatus (Tumeh), Palaquium sp., Dyera Costulata, Ilex Cymosa, Dyospyros sp., and Calophyllum spp [21, 22]. The study site is relatively flat with an elevation that varies between 4 m and 157 m.

Rainfall is common throughout the year and varies from about 60 inches (150 cm) to over 180 inches (450 cm) per year. In most parts of Sabah, the wettest months occur during the North East Monsoon from October through February and the driest months during the South West Monsoon from March to September.

3.2. SAR and Ancillary Data

ALOS-2 PALSAR Quad-Pol data was acquired for study site on April 23, 2015, in single look complex (SLC) format at incident angle 30.85°. The study area was covered in two adjacent scenes as shown in Figure 2. Temperature, humidity, and precipitation acquired from the nearest weather station indicate the local weather conditions. Land cover of the study site was obtained from CIFOR Atlas for Borneo Island (https://www.cifor.org/map/atlas/). SRTM 30 m DEM of study site was acquired from EarthExplorer (https://earthexplorer.usgs.gov/).

3.3. Field Data

Reference data wer acquired through a 30-day field visit in the study site. This field visit was conducted from August 20, 2018, to September 21, 2018. A total 56 plots of dimensions 20 m × 20 m = 400 m^2 were sampled. However, only data from 54 plots were used for further analysis because data in 2 plot were incomplete. The spatial distributions of sample plots are shown in Figure 2.

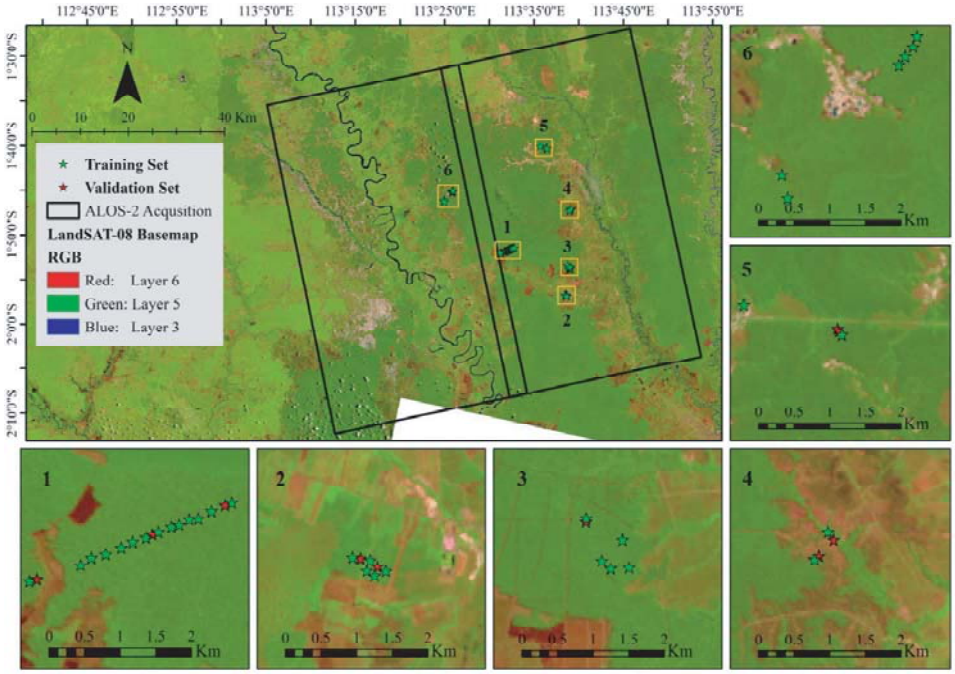

Figure 2. Spatial distribution of field data.

In each plot, biophysical parameters of the individual tree were measured, including diameter at breast height (DBH), tree species, and plot center GPS location. Due to existence of wild life and limited available resources, field data were only collected over easily accessible forest patches.

3.3.1. Data Cleaning — Removing Outliers

As Kalimantan forest mainly regrew and was logged during past 40–50 years, almost all age groups are present in sampled plots. The variability of DBH in individual plots is shown in Figure 4(a). It can be seen from Figure 4(a), DBH ranges from 2.55 cm to 150 cm. Locally developed allometric equations are listed in Table 1. Biomass is computed using all allometric equations listed in Table 1. A comparison of biomass estimated from locally developed allometric equations and generic allometric equation developed by Chave [52] is shown in Figure 3. However, biomass using allometric equations developed by [23] was chosen due to following two reasons: 1) This allometric equations is developed for mix species in central Kalimantan, 2) its estimation is close to the one estimated by generic allometric equation. Then plot-based AGB is calculated by aggregating biomass of all trees in each sample plot. Later, plot-based biomass is upscaled to 1 hectare scale by multiplying it with upscaling factor x (in our case, $x = 25$). As we are upscaling biomass estimated in 20 m × 20 m plot to 1 hectare scale, it is important to address outliers that exist in individual plot. In this research, we only consider DBH for forest AGB estimation; however if tree height is also available, more precise forest AGB estimation can be performed.

A few outliers will affect the estimated plot-based biomass and later introduce significant over-/under-estimation in reference field aboveground biomass data. In this research, outliers were removed from data by using inter-quartile range (IQR). Using Equation (23), outliers were removed from field

Table 1. Locally developed allometric equations for mix forest. Where St, Br, Tw, Le and WSG are Stem, Branch, Twing, Leaf and wood specific gravity respectively.

Allometric Model	Sample	Tree Component	DBH (cm)	R^2	Reference
$\ln\text{AGB} = -3.408 + 2.708 * \ln D$	40	St	1.1–115	0.98	[24]
$\text{AGB} = 2.708 * D^{2.486}$	bda	St	2–35	0.90	[25]
$\ln\text{AGB} = -2.26 + 1.27 * \ln D^2$	184	St	4.8–69.7	0.99	[23]
$\ln\text{AGB} = -4.26 + 1.36 * \ln D^2$	184	Br + Tw	4.8–69.7	0.91	[23]
$\ln\text{AGB} = -3.86 + 1.01 * \ln D^2$	184	Le	4.8–69.7	0.81	[23]
$\ln\text{AGB} = 1.201 + 2.196 * \ln(D)$	122	St	6.5–200	0.96	[26]
$\ln\text{AGB} = -0.744 + 2.188 * \log(D) + 0.832 * \log(\text{WSG})$	122	St	6.5–200	0.97	[26]
$\ln\text{AGB} = -2.289 + 2.649 * \ln(D) - 0.021 * \ln(D)^2$	226	St	5–148	0.98	[27]
$\text{AGB} = 42.69 - 12.8(D) + 1.242(D^2)$	170	St	5–148	0.84	[28]

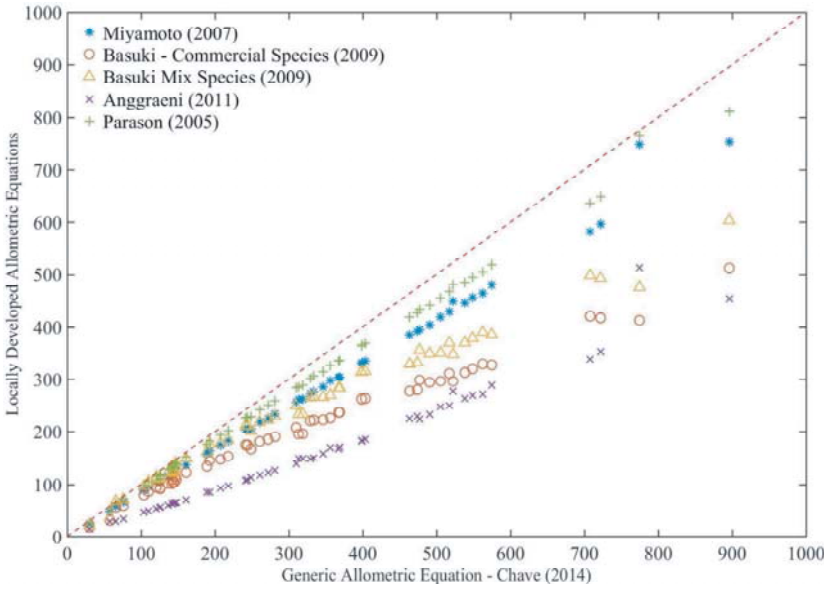

Figure 3. Biomass estimation using locally developed allometric equations vs generic allometric equation by Chave (2014) [23].

data, where Q_1 and Q_3 are the first and third quartiles, respectively. The distributions of DBH in individual plot before and after removing outliers are shown in Figure 4.

$$IQR = Q_3 - Q_1; \quad Q_3 + 1.5IQR < \text{Outlier} < Q_1 - 1.5IQR \tag{23}$$

Similarly, the distribution of resultant biomass, calculated using [23] is shown in Figure 4(c).

3.4. PolSAR Data Processing

Single Look Complex (SLC) data of the study site were acquired from JAXA. The data were polarimetrically calibrated by JAXA [15]. These data were multi-looked to get 5 meter square pixel size in resultant image. Backscattering coefficients for HH, HV, VH, and VV channels were estimated using Equation (17). Yamaguchi decomposition parameters (surface and volumetric scattering power) were computed using Equation (9). Eigen decomposition parameters, i.e., alpha (α), entropy, and

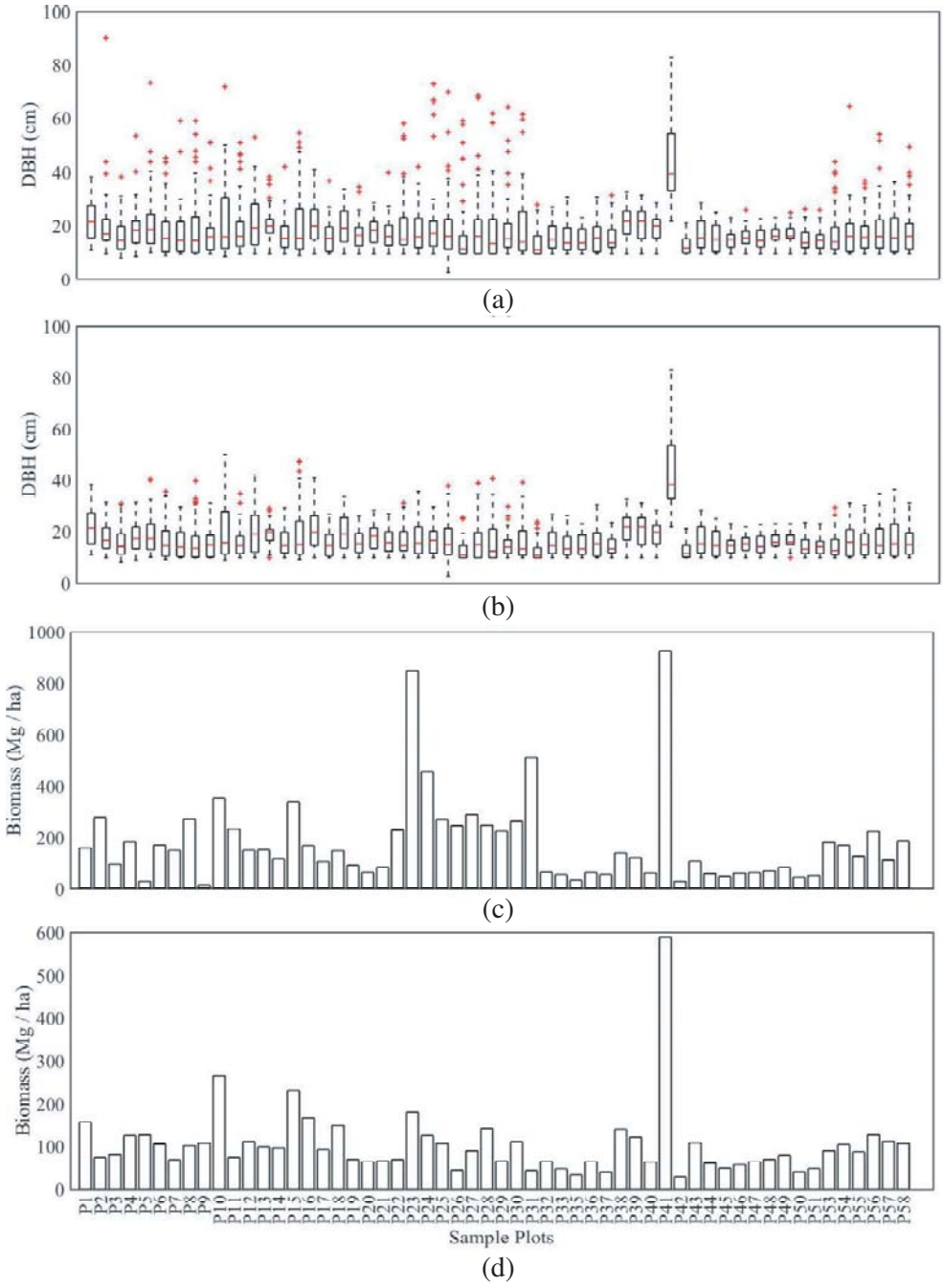

Figure 4. Boxplot representation. (a) Distribution of AGB in sampled plots. (b) Distribution of AGB in sampled plot after removing outliers.

anisotropy were computed using Equations (11), (15), and (16), respectively. Similarly, diversity indices were computed using Equations (18), (19), (20), (21), and (22), respectively. The whole processing was done using PolSARpro provided by European Space Agency (ESA) and PCI Geomatica. All of the computed parameters were terrain corrected, and lee sigma 5×5 speckle filter was applied to smoothen the speckles in the image. All of the computed parameters for further analysis are listed in Table 2.

For all the sample plots, 1×1 hectare mask was generated, and pixels under each mask were extracted for computed parameters listed in Table 2; also mean value of all extracted pixels corresponding to sample plot was computed. Regression analysis was performed between upscaled 1

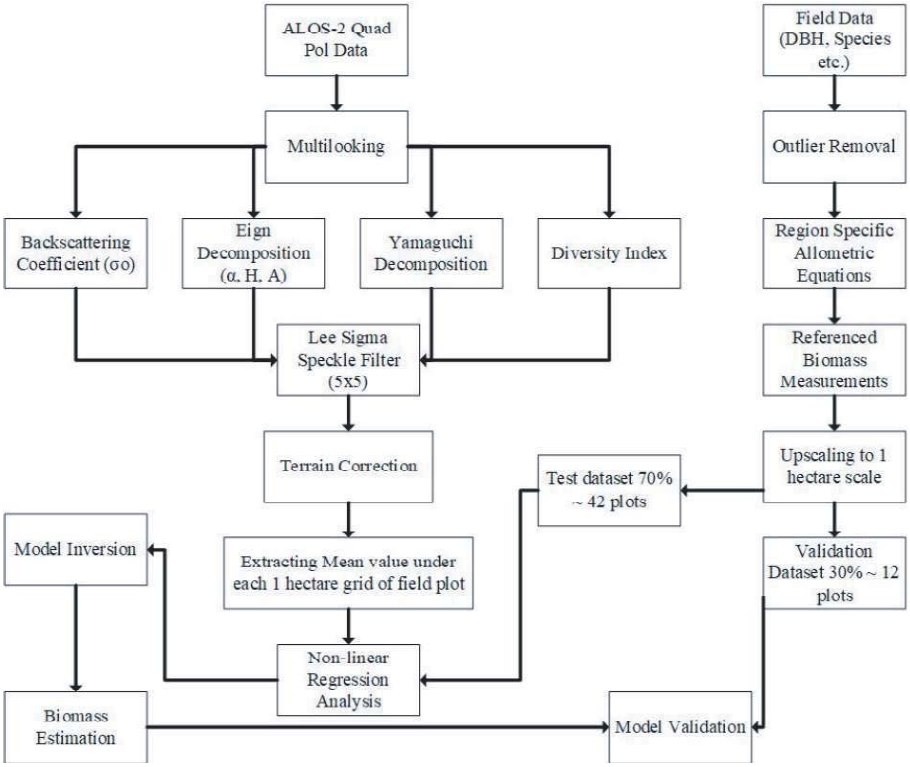

Figure 5. Methodological framework.

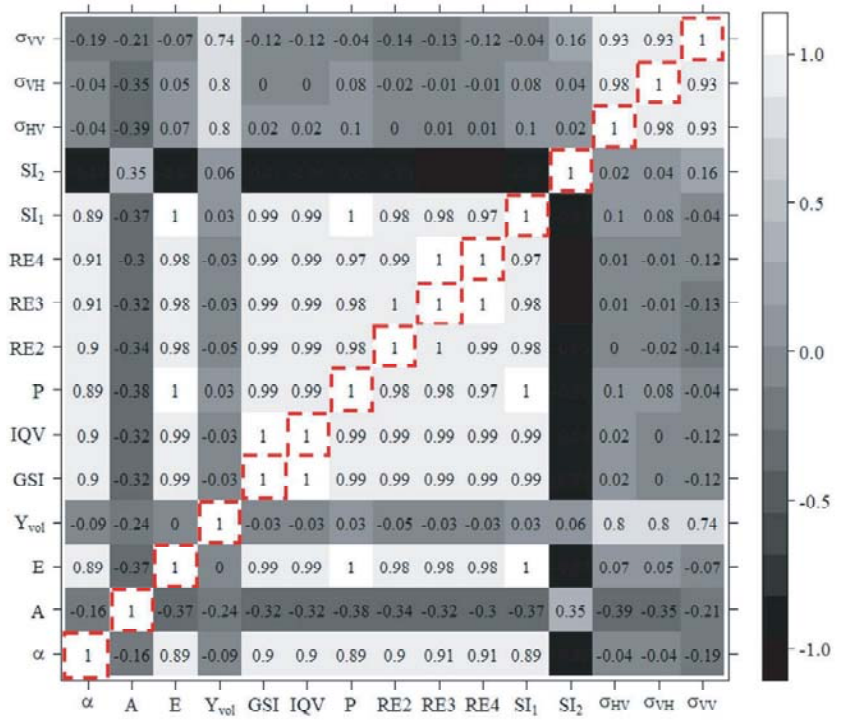

Figure 6. Correlation matrix between polarimetric parameters.

Table 2. Polarimetric parameters extracted from ALOS PALSAR-2.

Polarimetric Parameters		Description
σ_{HH}		Backscatter Coefficient of HH Channel
σ_{HV}		Backscatter Coefficient of HV Channel
σ_{VH}		Backscatter Coefficient of VH Channel
σ_{VV}		Backscatter Coefficient of VV Channel
$\sigma_{HH/HV}$		Backscatter Coefficient of HH/HV ratio
$\sigma_{VV/VH}$		Backscatter Coefficient of VV/VH ratio
Eigen Decomposition [29]	E	Scattering Entropy
	Alpha (α)	Scattering Mechanism
	A	Anisotropy
Yamaguchi Decomposition [13]	γ_s	Surface Scattering
	γ_d	Double Bounce Scattering
	γ_v	Volume Scattering
Diversity Index [30]	GSI	Gini Simpson Index
	IQV	Inverse Qualitative Inversion
	P	Perplexity
	RE2	Reyni Entropy (order $n = 2$)
	RE3	Reyni Entropy (order $n = 3$)
	RE4	Reyni Entropy (order $n = 4$)
	SI_1	Shannon Index
	SI_2	Simpson Index

Table 3. Biomass estimation models based on regression analysis between ground data and polarimetric parameters.

Parameter	Model $Y = a + b * \log(x)$		R^2	RMSE
Y	a	b		
Perplexity	1.998	0.1009	0.67	0.0417
Shannon Index (SI_1)	0.6924	0.0285	0.67	0.0118
Entropy (E)	0.6774	0.03188	0.66	0.0134
Gini Simpson Index	0.4599	0.01829	0.62	0.0084
Index of Qualitative Inversion	0.6924	0.02686	0.62	0.0125
Reyni Entropy (order 2)	0.2858	0.09595	0.61	0.0455
σ_{HV}	-24.88	2.846	0.57	1.4424
Alpha (α)	35.48	1.557	0.56	0.8135
σ_{VV}	-18.07	2.241	0.55	1.1835
γ_{vol}	87.95	2.052	0.49	1.2293

hectare referenced biomass measurements and corresponding mean values of all computed parameters. The regression results are shown in Table 3 and Figure 7. Among 56 sample plots collected during the field visit, data in two plots were not complete; those three plots were deleted from sampled data. Among reaming 54 plots, 42 were used as training plots for regression, and 12 plots were used for model validation.

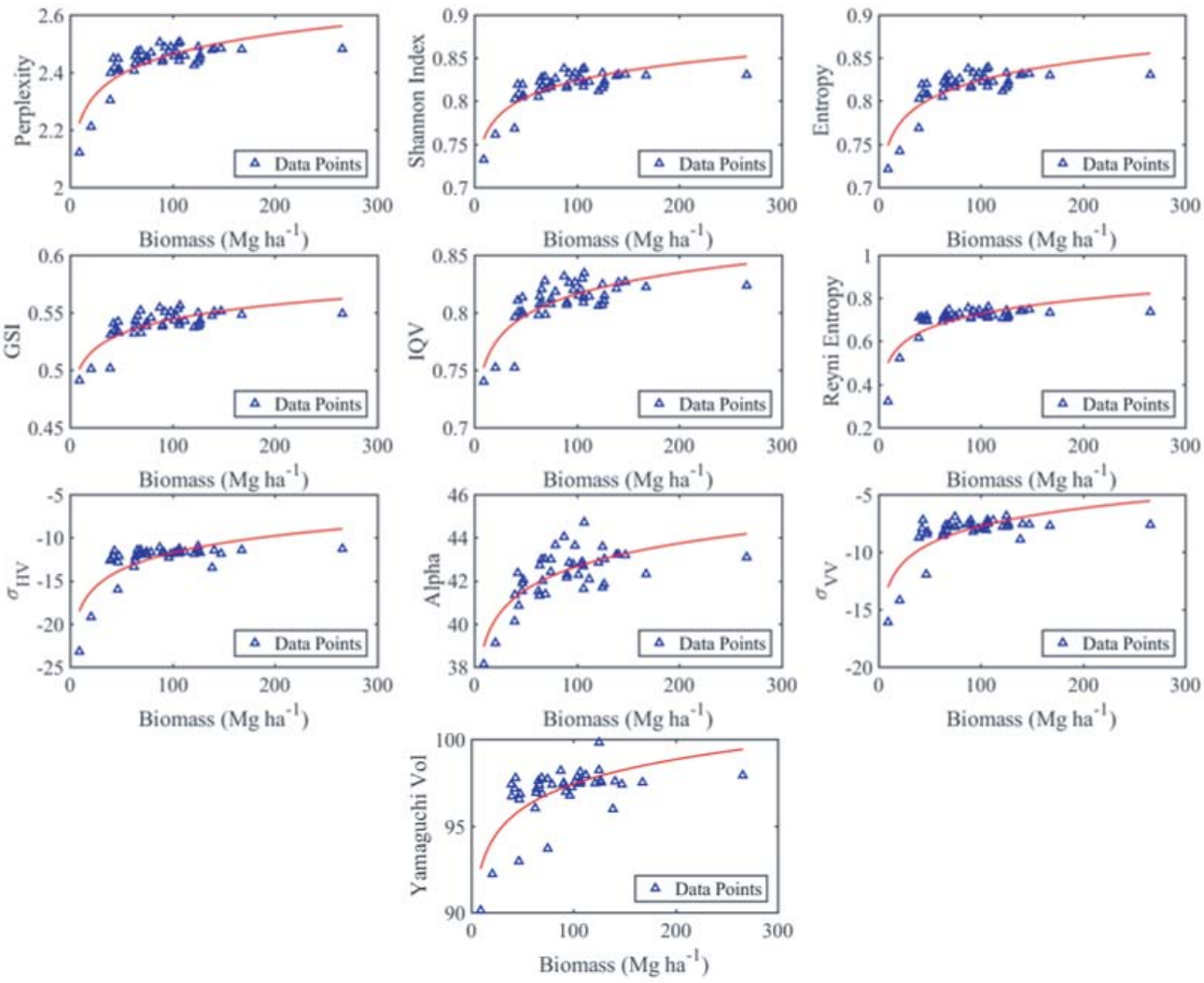

Figure 7. ALOS-2 based polarimetric parameters plotted against biomass ($n = 42$) and fitted popwer model.

The relationship between parameters extracted from ALOS-2 quad-pol data and referenced aboveground biomass was modeled using a logarithmic regression Equation (24). The accuracy of such a model is significantly influenced beyond the saturation point.

$$Y = a_o + a_1 \ln X \tag{24}$$

where X = aboveground forest biomass in Mgha^{-1}, Y = parameters extracted from SAR data, ln = natural log base e, a_o and a_1 are regression coefficients. For such models, model inversion needs to be performed to get biomass estimation models. The detailed methodological framework is shown in Figure 5.

4. RESULTS AND DISCUSSION

The correlation matrix among all computed polarimetric parameters is shown in Figure 6.

This matrix explains the relative importance of considered parameters for biomass estimation. From Figure 6, it can be seen that Shannon Index, Reyni Entropy, Perplexity, IQV, and GSI are highly correlated. It means that if we select only one parameter among these parameters, that can be the representative of all.

A significant correlation was found among diversity indices (perplexity, Shannon index, Gini Simpson index, index of qualitative inversion, and Reyni Entropy), polarimetric parameters (volumetric scattering power, alpha (α), and entropy), and backscattering coefficient (σ_{HV}, σ_{VV}) with referenced biomass measurements.

Among available variables, perplexity, Shannon index, and entropy were found most correlated with the referenced aboveground biomass with R^2 0.67, 0.67, and 0.66, respectively; these results are in line with the results obtained in published literature [31–36]. Detailed regression results are shown in Table 3. Using the regression model listed in Table 3, model inversion was performed to get the biomass estimation model. By using resultant models, biomass maps were generated using the individual inverted model.

The regression results for backscatter coefficient (σ), polarimetric parameters, diversity indices, and referenced aboveground biomass are shown in Figure 7. The initial aboveground biomass generated

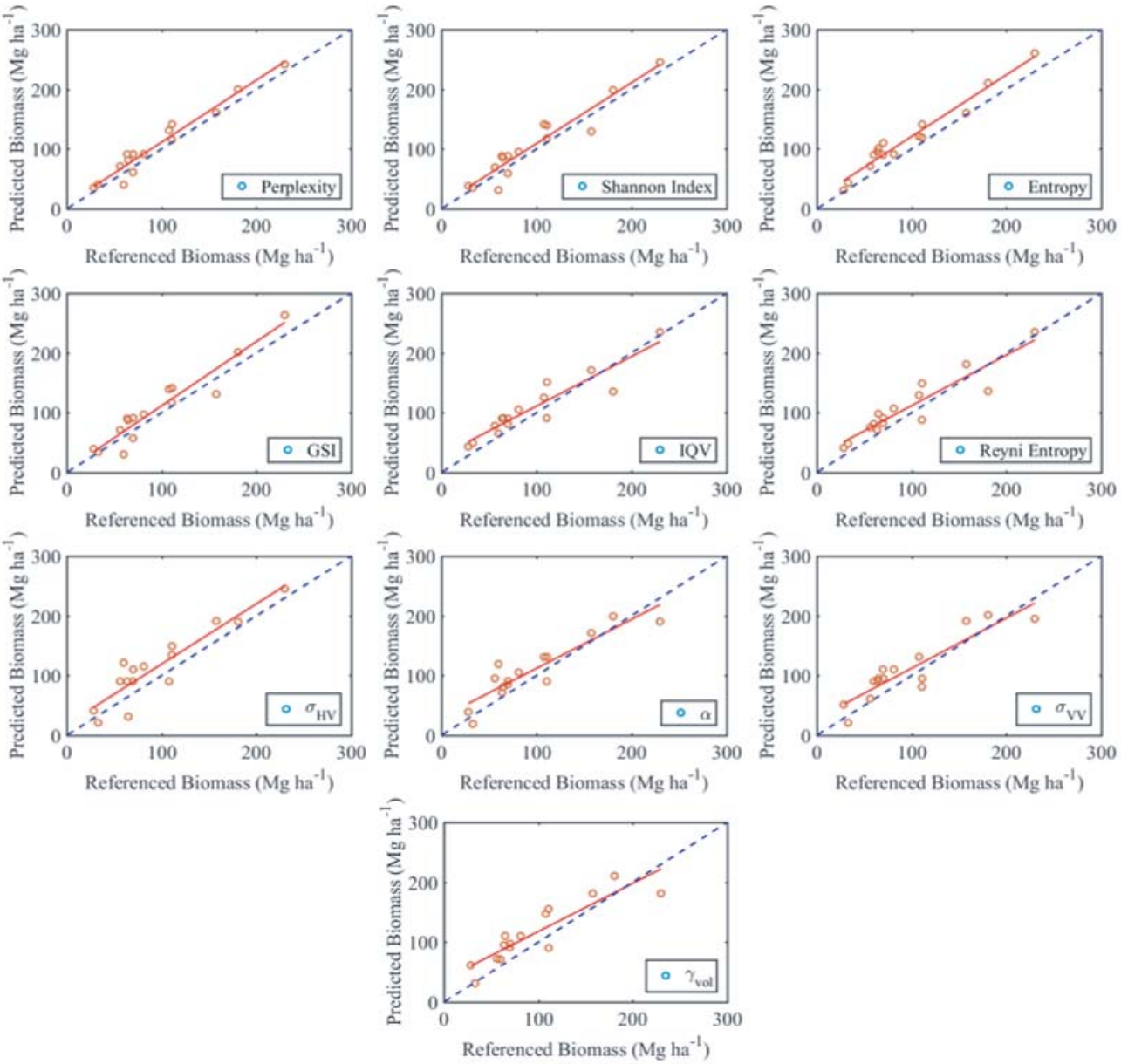

Figure 8. Model validation — Regression results between referenced and predicted biomass measurements, total 12 sampled referenced biomass measurements were used for validation.

maps were thresholded to remove unrealistic high values, and a low-pass smoothing filter was applied to remove further outliers. The generated biomass maps were validated using the validation set of referenced biomass measurements ($n = 12$), where 'n' is the number of validation data points. The validation results are shown in Figure 8. From Figure 8, it can be seen that predicted biomass using perplexity is higher compared to referenced measurements values; however, R^2 is 0.95 with RMSE 13.59 Mgha^{-1}. Similarly, Shannon Index, Entropy, GSI, and σ_{HV} overestimate biomass compared with referenced measurement. Also, validation results for biomass estimation using IQV, Reyni Entropy, Alpha (α), and σ_{VV} are also promising with reference measurement; however, for low biomass region predicted values are over estimated, and for higher biomass region predicted biomass is underestimated. The validation results are promising with reference to the field data with root mean square error (RMSE) ranging from 12.87 to 25.63 Mgha^{-1}. Validation results are summarized in Table 4.

Table 4. Forest biomass estimation with accuracy estimates.

Parameter	R^2	RMSE (Mgha^{-1})
Perplexity	0.95	13.59
Entropy	0.95	12.87
Shannon Index	0.90	19.28
GSI	0.90	20.34
IQV	0.86	18.99
Reyni Entropy	0.86	19.96
σ_{HV}	0.84	25.63
α	0.82	22.21
σ_{VV}	0.81	23.48
γ_{vol}	0.81	23.48

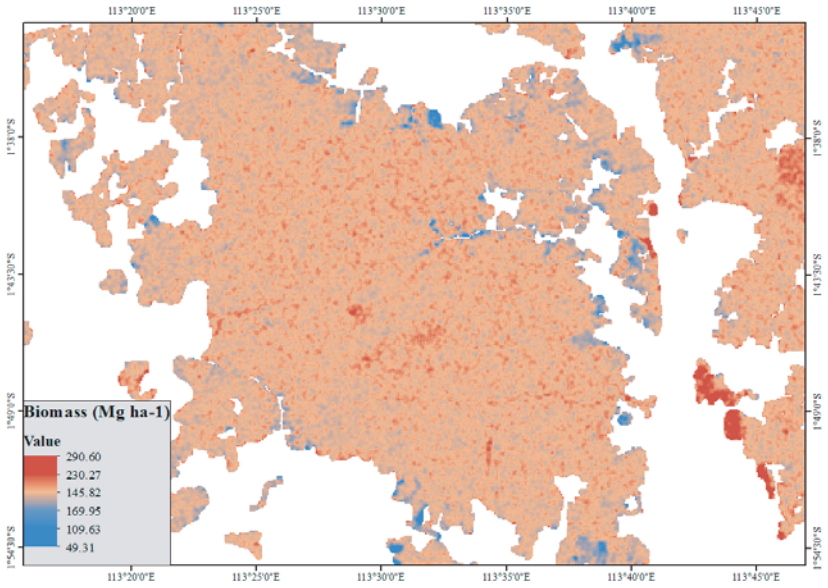

Figure 9. Forest biomass distribution in study area.

Biomass map of study area generated using perplexity model is shown in Figure 9. It can be seen that most of the region has an average biomass ranging from 140 Mgha^{-1} to 200 Mgha^{-1}. However, a few regions have higher biomass region with the maximum value of 290.60 Mgha^{-1} and minimum value of 49.31 Mgha^{-1}. Although the regression results are significant, due to the nonuniform distribution

of sample referenced plots in the study site, the proposed model is limited to biomass region with an average biomass ranging from $50\,\mathrm{Mgha}^{-1}$ to $300\,\mathrm{Mgha}^{-1}$.

4.1. Limitations

In this research, accurate forest aboveground biomass was accurately estimated with following limitations:

(i) As we can see, the referenced field measurements are uniformly distributed throughout the study area, and more referenced field measurements are needed to get a more accurate local biomass map. Furthermore, the allometric equations used in this study area are generic regional allometric equations; to get a more precise biomass map, species specific allometric equations are needed.

(ii) As region specific tree species allometric equations were not available, we have used regional allometric equations. However, tree species specific allometric equations can provide more accurate biomass estimation.

(iii) As explained by [50], L-band SAR signal saturates at $250\,\mathrm{Mgha}^{-1}$. However, most of the field based biomass measurements used are under $200\,\mathrm{Mgha}^{-1}$, and only one measurement is over $200\,\mathrm{Mgha}^{-1}$. Higher field based measurements are needed to precisely identify saturation point in this study.

5. CONCLUSIONS

This study presents tropical peatland forest aboveground biomass estimation using polarimetric parameters, diversity indices, and backscatter coefficient extracted using L-band ALOS PALSAR-2 dataset. A detailed methodology for preprocessing and extracting parameters is explained, and the parameters sensitives to aboveground biomass are identified by performing regression analysis of selected parameters with referenced field measurements. The referenced field data was divided into training (70 percent; $n = 42$) and validation (30 percent; $n = 12$) set. The validation set of referenced measurement was used to validated generated biomass, and acceptable R^2 was achieved. The reported RMSE ranged from $13.59\,\mathrm{Mgha}^{-1}$ to $23.48\,\mathrm{Mgha}^{-1}$.

This study will benefit in the further development of region-specific high-resolution biomass maps. However, more field-based referenced plot measurements are needed with relatively uniformly distributed and covering dominating forest species and density class in the study site.

Kalimantan Island, also called the lungs of Asia, has now become a very prominent study area for researchers around the world, and recently many efforts have been made for aboveground biomass estimation using optical, SAR, and lidar. Most of the studies using SAR and lidar are region specific, and these studies only consider biomass estimation modeling using backscatter information using X-, C- and L-band SAR. However, there is a need to investigate more advanced polarimetric parameters to have an in-depth understanding of biomass potential in the region.

ACKNOWLEDGMENT

Josaphat Laboratory (JMRSL) is supported in part by the 4th Japan Aerospace Exploration Agency (JAXA) ALOS Research Announcement under Grant 1024; the 6th JAXA ALOS Research Announcement under Grant 3170; Chiba University Strategic Priority Research Promotion Program FY2016-FY2018; SOAR-EI Canadian Space Agency (CSA) Project number 5436 FY2017-FY2019. JMRSL would like to acknowledge the support of PCI Geomatica for providing their software for this research.

REFERENCES

1. Cannell, M. G., *World Forest Biomass and Primary Production Data*, Academic Press, London, 1982.

2. Zhu, X. and D. Liu, "Improving forest aboveground biomass estimation using seasonal landsat NDVI time-series," *ISPRS Journal of Photogrammetry and Remote Sensing*, Vol. 102, 222–231, 2015.
3. Zhao, P., D. Lu, G. Wang, et al., "Examining spectral reflectance saturation in landsat imagery and corresponding solutions to improve forest aboveground biomass estimation," *Remote Sensing*, Vol. 8, No. 6, 469, 2016.
4. Karlson, M., M. Ostwald, H. Reese, et al., "Mapping tree canopy cover and aboveground biomass in Sudano-Sahelian woodlands using landsat 8 and random forest," *Remote Sensing*, Vol. 7, No. 8, 10017–10041, 2015.
5. Mutanga, O., E. Adam, and M. A. Cho, "High density biomass estimation for wetland vegetation using worldview-2 imagery and random forest regression algorithm," *International Journal of Applied Earth Observation and Geoinformation*, Vol. 18, 399–406, 2012.
6. Mitchard, E. T., S. S. Saatchi, I. H. Woodhouse, et al., "Using satellite radar backscatter to predict above-ground woody biomass: A consistent relationship across four different African landscapes," *Geophysical Research Letters*, Vol. 36, No. 23, 2009.
7. Qazi, W. A., S. Baig, H. Gilani, et al., "Comparison of forest aboveground biomass estimates from passive and active remote sensing sensors over Kayar Khola watershed, Chitwan district, Nepal," *Journal of Applied Remote Sensing*, Vol. 11, No. 2, 026038, 2017.
8. Baig, S., W. Qazi, A. M. Akhtar, et al., "Above ground biomass estimation of Dalbergia sissoo forest plantation from dual-polarized ALOS-2 PALSAR data," *Canadian Journal of Remote Sensing*, 2017, doi: 10.1080/07038992.2017.1330143.
9. Neumann, M., S. S. Saatchi, L. M. Ulander, et al., "Assessing performance of L- and P-band polarimetric interferometric SAR data in estimating boreal forest above-ground biomass," *IEEE Transactions on Geoscience and Remote Sensing*, Vol. 50, No. 3, 714–726, 2012.
10. Drake, J. B., R. G. Knox, R. O. Dubayah, et al., "Above-ground biomass estimation in closed canopy neotropical forests using lidar remote sensing: Factors affecting the generality of relationships," *Global Ecology and Biogeography*, Vol. 12, No. 2, 147–159, 2003.
11. Urbazaev, M., C. Thiel, F. Cremer, et al., "Estimation of forest aboveground biomass and uncertainties by integration of field measurements, airborne lidar, and SAR and optical satellite data in Mexico," *Carbon Balance and Management*, Vol. 13, No. 1, 5, 2018.
12. Shao, Z. and L. Zhang, "Estimating forest aboveground biomass by combining optical and SAR data: A case study in Genhe, Inner Mongolia, China," *Sensors*, Vol. 16, No. 6, 834, 2016.
13. Yamaguchi, Y., T. Moriyama, M. Ishido, et al., "Four-component scattering model for polarimetric SAR image decomposition," *IEEE Transactions on Geoscience and Remote Sensing*, Vol. 43, No. 8, 1699–1706, 2005.
14. Cloude, S. R. and E. Pottier, "A review of target decomposition theorems in radar polarimetry," *IEEE Transactions on Geoscience and Remote Sensing*, Vol. 34, No. 2, 498–518, 1996.
15. Shimada, M., O. Isoguchi, T. Tadono, et al., "Palsar radiometric and geometric calibration," *IEEE Transactions on Geoscience and Remote Sensing*, Vol. 47, No. 12, 3915–3932, 2009.
16. Shimada, M., M. Watanabe, T. Moriyama, et al., "Palsar radiometric and geometric calibration," *Journal of the Remote Sensing Society of Japan*, Vol. 27, No. 4, 308–328, 2007.
17. Motohka, T., O. Isoguchi, M. Sakashita, et al., "Results of ALOS-2 PALSAR-2 calibration and validation after 3 years of operation," *IGARSS 2018 — 2018 IEEE International Geoscience and Remote Sensing Symposium*, 4169–4170, IEEE, 2018.
18. Takahashi, H., "Estimation of ground water level in a peat swamp forest as an index of peat/forest fire," *Proceedings of the International Symposium on Land Management and Biodiversity in Southeast Asia*, Bali, Indonesia, September 2002.
19. Tawaraya, K., Y. Takaya, M. Turjaman, et al., "Arbuscular mycorrhizal colonization of tree species grown in peat swamp forests of central Kalimantan, Indonesia," *Forest Ecology and management*, Vol. 182, Nos. 1–3, 381–386, 2003.

20. Page, S. E., R. Wűst, D. Weiss, et al., "A record of late pleistocene and holocene carbon accumulation and climate change from an equatorial peat bog (Kalimantan, Indonesia): Implications for past, present and future carbon dynamics," *Journal of Quaternary Science*, Vol. 19, No. 7, 625–635, 2004.
21. Tuah, S. J., Y. M. Jamal, and S. H. Limin, "Nutritional characteristics in leaves of plants native to tropical peat swamps and heath forests of central Kalimantan, Indonesia," *Tropics*, Vol. 12, No. 3, 221–245, 2003.
22. Segah, H., H. Tani, and T. Hirano, "Detection of fire impact and vegetation recovery over tropical peat swamp forest by satellite data and ground-based NDVI instrument," *International Journal of Remote Sensing*, Vol. 31, No. 20, 5297–5314, 2010.
23. Miyamoto, K., J. S. Rahajoe, T. Kohyama, et al., "Forest structure and primary productivity in a bornean health forest," *Biotropica*, Vol. 39, No. 1, 35–42, 2007.
24. Anggraeni, B. W. and I. R. H. Purwanto, "Model pendugaan cadangan biomassa dan karbon hutan tropis basah di PT Sari Bumi Kusuma, Kalimantan Tengah," PhD thesis, Universitas Gadjah Mada, 2011.
25. Jaya, A., U. J. Siregar, H. Daryono, et al., "Biomasa hutan rawa gambut tropika pada berbagai kondisi penutupan lahan," *Jurnal Penelitian Hutan dan Konservasi Alam*, Vol. 4, No. 4, 341–352, 2007.
26. Basuki, T., P. Van Laake, A. Skidmore, et al., "Allometric equations for estimating the above-ground biomass in tropical lowland dipterocarp forests," *Forest Ecology and Management*, Vol. 257, No. 8, 1684–1694, 2009.
27. Pearson, T., S. Walker, and S. Brown, "Sourcebook for land use, land-use change and forestry projects," World Bank, Washington, DC, 2013.
28. Brown, S., *Estimating Biomass and Biomass Change of Tropical Forests: A Primer*, Vol. 134, Food & Agriculture Org., 1997.
29. Mitchard, E. T., S. S. Saatchi, I. H. Woodhouse, et al., "Using satellite radar backscatter to predict above-ground woody biomass: A consistent relationp across four different African landscapes," *Geophysical Research Letters*, Vol. 36, No. 23, 2009.
30. He, F. and X.-S. Hu, "Hubbell's fundamental biodiversity parameter and the simpson diversity index," *Ecology Letters*, Vol. 8, No. 4, 386–390, 2005.
31. Antropov, O., Y. Rauste, T. Häme, et al., "Polarimetric alos palsar time series in mapping biomass of boreal forests," *Remote Sensing*, Vol. 9, No. 10, 999, 2017.
32. Cougo, M. F., P. W. Souza-Filho, A. Q. Silva, et al., "Radarsat-2 backscattering for the modeling of biophysical parameters of regenerating mangrove forests," *Remote Sensing*, Vol. 7, No. 12, 17097–17112, 2015.
33. Vaglio Laurin, G., F. Pirotti, M. Callegari, et al., "Potential of ALOS2 and NDVI to estimate forest above-ground biomass, and comparison with lidar-derived estimates," *Remote Sensing*, Vol. 9, No. 1, 18, 2017.
34. Morel, A. C., S. S. Saatchi, Y. Malhi, et al., "Estimating aboveground biomass in forest and oil palm plantation in Sabah, Malaysian Borneo using ALOS PALSAR data," *Forest Ecology and Management*, Vol. 262, No. 9, 1786–1798, 2011.
35. Kronseder, K., U. Ballhorn, V. Böhm, et al., "Above ground biomass estimation across forest types at different degradation levels in central Kalimantan using lidar data," *International Journal of Applied Earth Observation and Geoinformation*, Vol. 18, 37–48, 2012.
36. Englhart, S., J. Franke, V. Keuck, et al., "Aboveground biomass estimation of tropical peat swamp forests using SAR and optical data," *2012 IEEE International Geoscience and Remote Sensing Symposium (IGARSS)*, 6577–6580, IEEE, 2012.
37. Wagner, W., A. Luckman, J. Vietmeier, et al., "Large-scale mapping of boreal forest in SIBERIA using ERS tandem coherence and JERS backscatter data," *Remote Sensing of Environment*, Vol. 85, No. 2, 125–144, 2003.

38. Lucas, R., J. Armston, R. Fairfax, et al., "An evaluation of the ALOS PALSAR L-band backscatter — Above ground biomass relationship Queensland, Australia: Impacts of surface moisture condition and vegetation structure," *IEEE Journal of Selected Topics in Applied Earth Observations and Remote Sensing*, Vol. 3, No. 4, 576–593, 2010.
39. Englhart, S., V. Keuck, and F. Siegert, "Aboveground biomass retrieval in tropical forests — The potential of combined X- and L-band SAR data use," *Remote Sensing of Environment*, Vol. 115, No. 5, 1260–1271, 2011.
40. Imhoff, M. L., "Radar backscatter/biomass saturation: Observations and implications for global biomass assessment," *Proceedings of IGARSS'93, IEEE International Geoscience and Remote Sensing Symposium*, 43–45, IEEE, 1993.
41. Carreiras, J. M., M. J. Vasconcelos, and R. M. Lucas, "Understanding the relationship between aboveground biomass and ALOS PALSAR data in the forests of Guinea-Bissau (West Africa)," *Remote Sensing of Environment*, Vol. 121, 426–442, 2012.
42. Næsset, E., "Airborne laser scanning as a method in operational forest inventory: Status of accuracy assessments accomplished in Scandinavia," *Scandinavian Journal of Forest Research*, Vol. 22, No. 5, 433–442, 2007.
43. Dobson, M. C., F. T. Ulaby, T. LeToan, et al., "Dependence of radar backscatter on coniferous forest biomass," *IEEE Transactions on Geoscience and remote Sensing*, Vol. 30, No. 2, 412–415, 1992.
44. Le Toan, T., S. Quegan, M. Davidson, et al., "The biomass mission: Mapping global forest biomass to better understand the terrestrial carbon cycle," *Remote Sensing of Environment*, Vol. 115, No. 11, 2850–2860, 2011.
45. Van Con, T., N. T. Thang, C. C. Khiem, et al., "Relationship between aboveground biomass and measures of structure and species diversity in tropical forests of Vietnam," *Forest Ecology and Management*, Vol. 310, 213–218, 2013.
46. Li, S., J. Su, X. Lang, et al., "Positive relationship between species richness and aboveground biomass across forest strata in a primary Pinus kesiya forest," *Scientific Reports*, Vol. 8, No. 1, 2227, 2018.
47. Dossa, G. G., E. Paudel, J. Fujinuma, et al., "Factors determining forest diversity and biomass on a tropical volcano, Mount Rinjani, Lombok, Indonesia," *PloS One*, Vol. 8, No. 7, 67720, 2013.
48. Li, S., X. Lang, W. Liu, et al., "The relationship between species richness and aboveground biomass in a primary Pinus kesiya forest of Yunnan, Southwestern China," *PloS One*, Vol. 13, No. 1, 0191140, 2018.
49. Day, M., C. Baldauf, E. Rutishauser, et al., "Relationships between tree species diversity and above-ground biomass in central African rainforests: Implications for REDD," *Environmental Conservation*, Vol. 41, No. 1, 64–72, 2014.
50. Lucas, R., J. Armston, R. Fairfax, et al., "An evaluation of the alos palsar L-band backscatter—above ground biomass relationship queensland, australia: Impacts of surface moisture condition and vegetation structure," *IEEE Journal of Selected Topics in Applied Earth Observations and Remote Sensing*, Vol. 3, No. 4, 576–593, 2010.
51. Miyamoto, K., J. S. Rahajoe, T. Kohyama, et al., "Forest structure and primary productivity in a bornean heath forest," *Biotropica*, Vol. 39, No. 1, 35–42, 2007.
52. Chave, J., M. Réjou-Méchain, A. Búrquez, et al., "Improved allometric models to estimate the aboveground biomass of tropical trees," *Global Change Biology*, Vol. 20, No. 10, 3177–3190, 2014.